Measurements of Impact Properties of Small, Nearly Spherical Particles

by A. Lorenz, C. Tuozzolo and M. Y. Louge

ABSTRACT—The authors report impact properties for collisions of small, nearly spherical particles that present interesting experimental challenges. They consider difficulties arising with surface reflectivity, slight asphericity, surface damage and collisions with particles affixed to a rigid plate. To measure these impact properties, the authors refine the experimental technique of Foerster *et al.* To permit straightforward incorporation in rapid granular theories, the impacts are described with three coefficients. The first is the Newtonian coefficient of normal restitution. The second represents the frictional properties of the contact surfaces. The last characterizes the restitution of the tangential component of the contact point velocity for impacts that involve negligible sliding.

Background

Flows of granular materials occur in industrial processes involving solid transport and in phenomena as diverse as avalanches, landslides and planetary ring formation. Although these flows generally combine several mechanisms of grain interaction, an important regime is where grains exchange momentum and energy through individual impacts. This regime is called rapid granular flows.[1] Theories of rapid granular flows are generally developed for spherical grains. They adopt a model for a collision between a pair of rigid spheres, then proceed to calculate the average properties of the flow using appropriate velocity distribution functions.

To keep the corresponding integrations tractable, these theories generally treat individual collisions using the simplified model of Walton[2] rather than describe the evolution of each impact in detail. Walton's model is based upon three constant impact coefficients that permit unambiguous determination of the linear and angular velocities of each sphere after impact. Before carrying out meaningful tests of a rapid granular theory that employs this impact model, it is essential to verify that the three impact coefficients provide an adequate description of the collision and, if so, determine their values. Unfortunately, because their measurement involves the precise control of the trajectories of small particles, these coefficients were seldom determined in the past.

In this context, Foerster *et al.*[3] described an experimental apparatus that measures the collision properties of spheres as small as 3 mm in diameter. Their apparatus included a mechanism that brought two identical particles into a collision without initial spin and a stroboscopic setup that photographed the dynamics of their flights. The setup could also produce impacts between a single sphere and a flat plate. In that paper, Foerster *et al.* reported impact coefficients for binary collisions of 3-mm glass and 6-mm cellulose acetate spheres and for collisions of these spheres with a thick, smooth, flat aluminum plate. They showed that Walton's model captures the behavior of the impact over a wide range of incident angles. Dave, Yu and Rosato[4] reached similar conclusions with impacts of two larger nylon spheres 25 mm in diameter. Massah *et al.*[5] employed this model to interpret the trajectories of 190-μm glass spheres and 90-μm fluid-cracking-catalyst particles impacting a flat wall in the considerably more complex environment of a wind tunnel.

The principal objective of the present paper is to report measurements in situations that eluded Foerster *et al.* In particular, we consider difficulties arising with surface reflectivity, slight asphericity, surface damage and collisions with spheres affixed to a rigid plate. We also report properties of binary collisions for other sphere materials commonly employed in granular experiments. We begin with a discussion of Walton's impact model and its limitations. We then describe the apparatus and discuss each series of experiments.

Impact Model

Consider rigid spheres of diameters σ_1 and σ_2, center of mass velocities c_1 and c_2, and spins ω_1 and ω_2 before impact (Fig. 1). The relative velocity of the contact point is

$$\mathbf{g} = (\mathbf{c}_1 - \mathbf{c}_2) - \left(\frac{\sigma_1}{2}\omega_1 + \frac{\sigma_2}{2}\omega_2\right) \times \mathbf{n}, \qquad (1)$$

where $\mathbf{n}$ is the unit normal vector joining the centers of the spheres at contact. The incident angle γ between $\mathbf{g}$ and $\mathbf{n}$ characterizes the impact geometry, $\cot\gamma \equiv \mathbf{g}.\mathbf{n}/|\mathbf{g} \times \mathbf{n}|$. Because impacts occur when $\mathbf{g}.\mathbf{n} \leq 0$, this angle lies in the range $\pi/2 \leq \gamma \leq \pi$.

The postcollision velocities are derived by writing the balance of linear and angular momenta in the collision and by invoking a closure that captures details of the impact process. Walton's closure is based on three constant impact coefficients.[2] The Newtonian coefficient of normal restitution e characterizes the incomplete restitution of the normal component of $\mathbf{g}$,

$$\mathbf{n}.\mathbf{g}' = -e\mathbf{n}.\mathbf{g}, \qquad (2)$$

A. Lorenz and C. Tuozzolo are Research Assistants, and M.Y. Louge is Associate Professor, Sibley School of Mechanical and Aerospace Engineering, Cornell University, Ithaca, NY 14853.

Original manuscript submitted: February 13, 1996.
Final manuscript received: January 21, 1997.

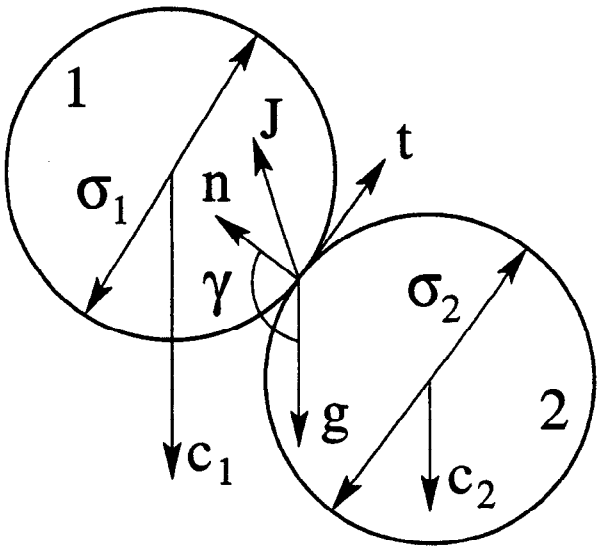

Fig. 1—Typical geometry of a binary collision projected on the collision plane. The velocities are shown before the impact

where $0 \leq e \leq 1$ and prime denotes conditions after the collision.

Grazing collisions with incident angles near $\pi/2$ involve gross sliding. For these, Walton assumes that sliding is resisted by Coulomb friction and that the tangential and normal components of the impulse **J** are related by the coefficient of friction μ,

$$|\mathbf{n} \times \mathbf{J}| = \mu(\mathbf{n}.\mathbf{J}), \tag{3}$$

where $\mu \geq 0$.

For greater values of the incident angle, the impact is closer to head on, and gross sliding is no longer involved as parts of the contact patch are brought to rest. When γ exceeds the limiting angle γ_0, Walton replaces eq (3) by

$$\mathbf{n} \times \mathbf{g}' = -\beta_0 \mathbf{n} \times \mathbf{g}, \tag{4}$$

where $\gamma_0 \equiv \pi - \text{atan}[7(1+e)\mu/2(1+\beta_0)]$ and β_0 is the tangential coefficient of restitution, with $0 \leq \beta_0 \leq 1$. For simplicity, he then categorizes the collision as "sticking" and assumes that the entire contact point is brought to rest during impact. For sticking collisions, the definition of β_0 in eq (4) implies that some of the elastic strain energy stored in the solid during impact is recoverable through tangential compliance, so the tangential velocity of the point of contact may be reversed. In this simple model, eqs (3) and (4) are mutually exclusive, i.e., the point of contact is either sliding [eq (3)] or sticking [eq (4)]. This distinction thus defines two separate impact regimes.

A convenient way to interpret data from an impact experiment is to follow Maw, Barber and Fawcett[6,7] and produce a plot of $\Psi_2 \equiv -(\mathbf{g}'.\mathbf{t})/(\mathbf{g}.\mathbf{n})$ versus $\Psi_1 \equiv -(\mathbf{g}.\mathbf{t})/(\mathbf{g}.\mathbf{n})$, where **t** is a unit vector located in the collision plane (**g**, **n**) and tangent to both spheres. In collisions of homogeneous spheres that involve gross sliding,

$$\Psi_2 = \Psi_1 - \frac{7}{2}(1+e)\mu \ \text{sign}(\mathbf{g}.\mathbf{t}), \tag{5}$$

and in collisions that do not,

$$\Psi_2 = -\beta_0 \Psi_1. \tag{6}$$

For positive values of $\mathbf{g}.\mathbf{t}$, Ψ_1 represents the magnitude of the tangent of the incident angle. Similarly, the ratio (Ψ_2/e) is the tangent of the recoil angle γ' between **n** and **g**′. In the plot of Ψ_2 versus Ψ_1, the data fall on two distinct straight lines [eqs (5) and (6)] that permit unambiguous identification of the sliding and sticking regimes. Foerster *et al.* provide a detailed derivation of those equations.[3]

However, because of its inherent simplicity, Walton's model possesses limitations for particles other than nearly rigid spheres. The principal problem is a failure of the concept of normal restitution coefficient for certain impact geometries. While addressing this issue, Smith and Liu[8] recall three definitions of this coefficient, each of which focuses on the partial restitution of a different mechanical quantity. The first, attributed to Newton, is the restitution of the normal component of the velocity at the contact point [eq (2)]. This kinematic approach is adequate for nearly rigid spheres undergoing small deformation of the contact patch but, as Smith[9] shows, it fails when the impact is not collinear, i.e., the normal at the contact point is not directed along the line joining the centers of mass of the two colliding particles. For certain pathological geometries, the Newtonian definition can even predict creation of kinetic energy in the impact, which violates the second law of thermodynamics.

The second definition of normal restitution circumvents the energy paradox. It focuses on the normal impulse, which represents the integral of the normal impact force over time. Here, the impact is divided into compression and restitution phases, separated by the instant when the relative contact velocity vanishes. Inelastic impacts recover only a part of the compression impulse during the restitution phase. Poisson's hypothesis is that the ratio of the two impulses is the coefficient of normal restitution. For two-dimensional impacts, this hypothesis leads naturally to Routh's graphical method, which provides a convenient description of the impact process.[10] Stronge[11] proposes a third definition, which equates the square of the coefficient of restitution to the ratio of the elastic strain energy released during restitution to that absorbed during compression.

For collinear impacts, the definitions of Newton, Poisson and Stronge are equivalent. Because the kinetic theory treats rapid granular flows using statistical distributions of grain velocities, it naturally incorporates a kinematic definition of normal restitution. Therefore, the Newtonian coefficient is the formalism that we adopt to report our experimental results. It remains to be established experimentally the significance of producing impacts with slight departures from collinearity.

Another limitation of Walton's model concerns tangential compliance. For spheres, tangential compliance leads to the possible reversal of the tangential component of the relative velocity at contact. However, as Maw, Barber and Fawcett[6,7] and Stronge[12] showed with an elastic continuum analysis and an inelastic lumped parameter model, respectively, the tangential coefficient of restitution in eq (4) becomes awkward in situations where the ratio Ψ_2/Ψ_1 is positive at low values of Ψ_1, i.e., with nearly head-on impacts. This situation is exacerbated at large Poisson's ratios and high elasticity.[12] Nevertheless, because head-on impacts occur infrequently in

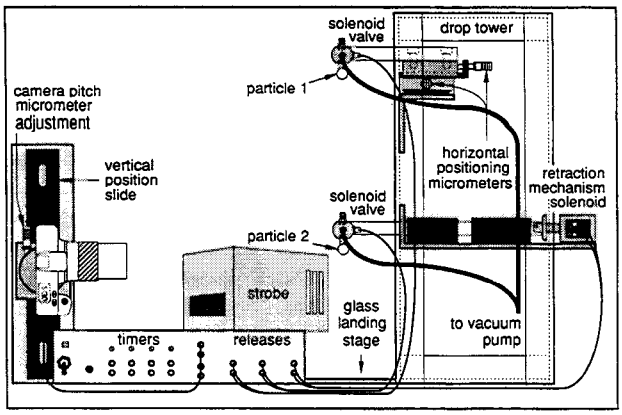

Fig. 2—Side perspective of the experimental apparatus. The particles are drawn to an exaggerated scale

rapid granular flows, the errors resulting from the assumption of a constant, positive β_0 are likely to remain inconsequential.

Apparatus and Procedure

The experimental apparatus of Foerster *et al.*[3] is sketched in Fig. 2. It consists of two mechanisms that release the small particles in a free fall. In a binary collision experiment, the top particle is dropped first from a height of 53.9 cm above the landing stage. At a later time, the bottom particle is liberated from a height of 27.9 cm, and its release mechanism is promptly retracted using a solenoid to permit the top particle to catch up and eventually collide. An electronic timing circuit coordinates the successive release of the top and bottom particles, the retraction of the lower release mechanism and the opening of the camera shutter. Calculations ensure that the particles collide near the center of the camera's field of view. Through stroboscopic illumination, a photographic camera records successive positions of the spheres before and after the collision.

In this work, we refine the experiment of Foerster *et al.*[3] by employing a Kodak DCS digital camera. This black-and-white system images the stroboscopic object on a CCD array of 20.5×16.4 mm,^{2} with individual pixel resolution of $16 \times 16\ \mu$m^2 up to an exposure index of 1600. Because it bypasses the conventional photographic process, the new camera simplifies the data processing considerably. By allowing rapid inspection of the image, it also permits immediate adjustment of the collision orientation.

The digitized pictures are analyzed using computer-aided design software. A circle is superimposed on each particle image to establish the location of its center. Because the collision has a very short duration, it is not captured on film. Instead, the position and velocity of each sphere at impact are extrapolated from two successive images on the photograph. From this extrapolation, we infer the unit normal $\mathbf{n}$ and the linear velocities before impact $\mathbf{c}_1$ and $\mathbf{c}_2$, and those following impact $\mathbf{c}_1'$ and $\mathbf{c}_2'$. This permits us to evaluate the collisional impulse

$$\mathbf{J} = m_1(\mathbf{c}_1' - \mathbf{c}_1) = -m_2(\mathbf{c}_2' - \mathbf{c}_2), \qquad (7)$$

where m_1 and m_2 are the masses of the two colliding spheres. By conservation of angular momentum at the contact point, we then infer the impulsive change in spin of each particle

$$(2I_1/\sigma_1)(\omega_1' - \omega_1) = (2I_2/\sigma_2)(\omega_2' - \omega_2) = (\mathbf{n} \times \mathbf{J}), \quad (8)$$

where $I = m\sigma^2/10$ is the moment of inertia about the center of a homogeneous sphere.

The principal feature of this apparatus is that it releases the particles reproducibly and without initial spin. Then, because $\omega_1 = \omega_2 = 0$, the postcollision spins ω_1' and ω_2' are calculated from measurements of $\mathbf{n}$ and linear velocities using eqs (7) and (8). In these experiments, it is therefore superfluous to measure spin directly, which is a far more difficult task for small particles than to record the linear velocities of their centers of mass. From known linear and angular velocities, we then calculate the relative velocities at contact $\mathbf{g}$ and $\mathbf{g}'$ and plot the corresponding values of Ψ_2 and Ψ_1. Foerster *et al.*[3] provide further details of the experimental apparatus and data analysis.

In this work, we measure impact properties in several situations that eluded Foerster *et al.* We now describe details of each series of experiments and discuss the corresponding results.

Reflective Spheres

The photographic technique of Foerster *et al.*[3] infers the location of the center of the falling spheres from the circular outline of their surface. It relies on diffuse reflection to obtain sharp photographic contrast and to distinguish the edge of the spheres without ambiguity. Figure 3 is a typical image with diffusely reflective particles. Spheres with strong specular reflection defeat this imaging technique. Because their surfaces reflect most stroboscopic light specularly, bright spots overwhelm the photographs and prevent their circular edges from being distinguished.

We resolve this difficulty by painting a portion of the spheres that is not involved in the collision with a fluorescent dye. The fluorescence produces bright diffuse regions that clearly highlight the circular outline of the spheres. Stainless steel spheres provide a convenient demonstration of this method. Figure 4 shows bright specular spots and regions of diffuse fluorescence. Edges of the latter also confirm that spin is negligible before impact and significant thereafter. The corresponding impact data are plotted in Fig. 5. Here, glancing impacts were recorded with values of Ψ_1 as large as 6.5. To show sticking collisions with clarity, we limit values of Ψ_1 represented in Fig. 5.

Slight Asphericity and Surface Damage

Foerster *et al.*[3] measured the impact properties of nearly perfect spheres. However, in experiments involving large numbers of grains, the cost of perfect monodisperse spheres is prohibitive. Slightly aspherical particles of relatively narrow size distribution are more affordable. In practical experiments, it remains to be established whether the collision model of eqs (5) and (6) stays valid despite slight departures from perfect sphericity and monodispersity exhibited by individual particles.

To answer this question qualitatively, we tested the binary collisions of randomly selected pairs of lead-free glass beads 3 mm in nominal diameter (Jaygo "Dragonite"). We inferred the mean bead diameter of 2.968 ± 0.020 mm from measurements of the mass of 10 beads and knowledge of their

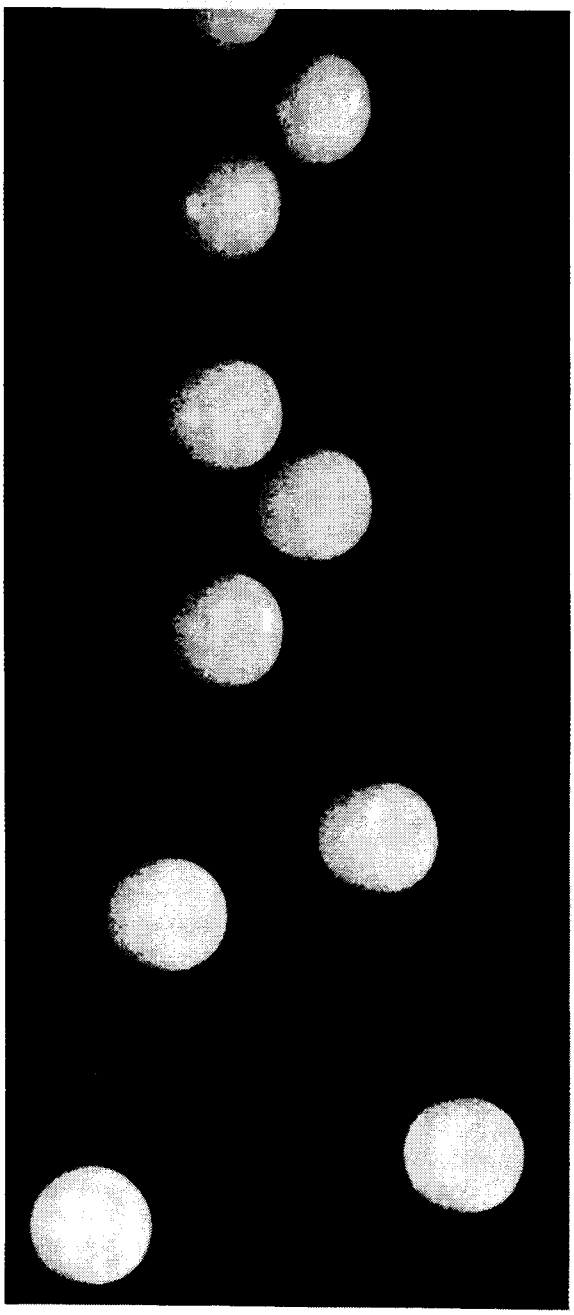

Fig. 3—Typical stroboscopic image showing the ballistic trajectories of two acrylic spheres before and after impact. In this experiment, $\Psi_1 = 1.103$ and $\Psi_2 = 0.492$

material density 2.50 ± 0.04 g/cc. We further characterized the asphericity of each of the 10 beads by recording their width along 20 random orientations using a micrometric dial caliper. On average, the relative excursion of the width was approximately 1.1 percent of the mean diameter of each bead. As Fig. 6(a) demonstrates, the random asphericity and size distribution appear as additional scatter in the data. Despite the scatter, it is still possible to extract meaningful impact parameters that may serve as convenient input to the granular theory.

Another practical problem is associated with surface damage. Because in a typical impact large forces are exerted on a small contact area for a short period, the particle surface often

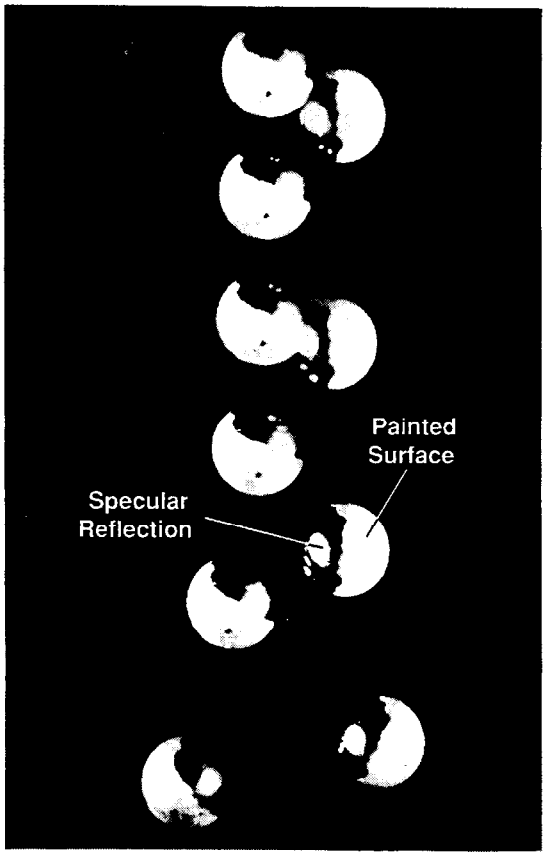

Fig. 4—Stroboscopic image of the binary collision of two 5-mm stainless steel spheres. In this experiment, $\Psi_1 = 1.156$ and $\Psi_2 = 0.546$

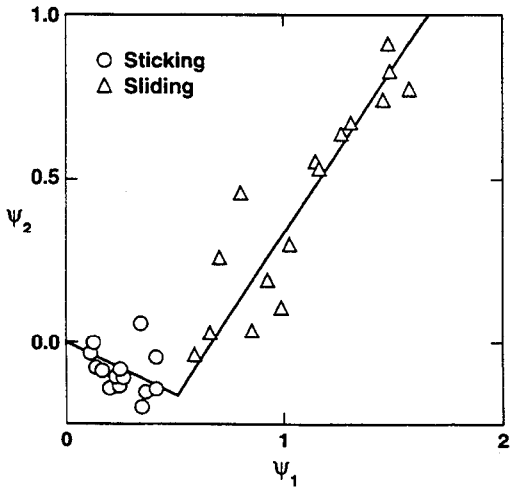

Fig. 5—Results for the binary impacts of two 5-mm stainless steel spheres. Solid lines are the best fit of eqs (5) and (6)

experiences microscopic dislocations that modify its macroscopic properties. Brittle materials such as glass are particularly subject to this gradual transformation. To demonstrate this effect qualitatively, we circulated large numbers of fresh 3-mm Jaygo glass beads in our chute facility for a combined period of at least 20 hours. In this facility, a conveyor belt recycles the glass beads continuously onto an inclined alu-

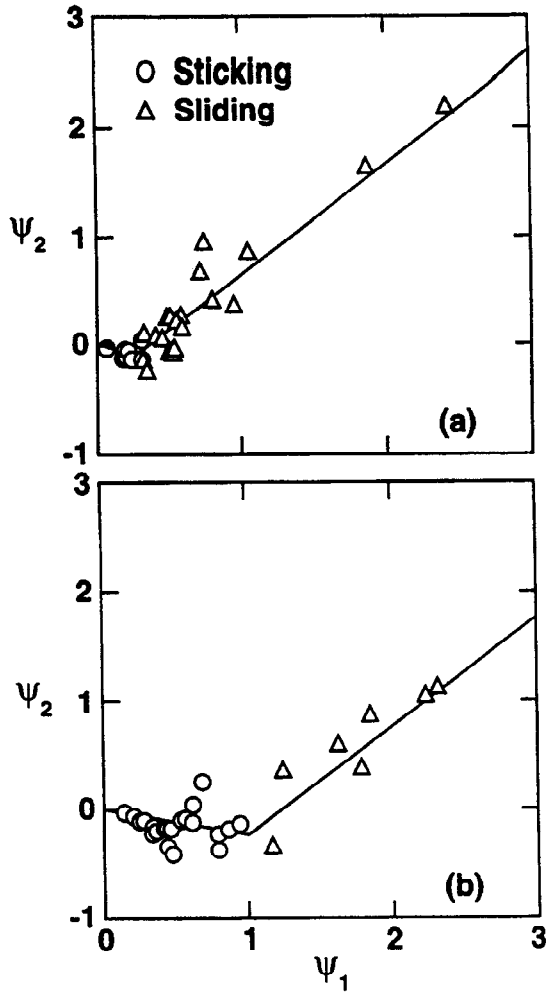

Fig. 6—Results for binary collisions of slightly aspherical glass beads 3 mm in nominal diameter: (a) fresh beads, (b) spent beads

minum plane. Emissions of microscopic glass dust rapidly became evident. However, because the general shape of the beads remained unchanged, the damage was probably limited to the particle surface. As Fig. 6(b) illustrates, collision tests of the "spent" beads revealed changes in binary impact properties primarily related to surface friction. In particular, it is clear from Fig. 6 that the transition between sticking and sliding contacts occurred at a larger value of Ψ_1 for the spent beads.

Similarly, prolonged granular flow experiments exert considerable microscopic damage to the bottom aluminum surface of the chute. To substantiate this transformation, we collided spent glass beads with a sample of the damaged aluminum surface and compared the results with fresh beads impacting a smooth plate. We observed a small increase in the coefficient of friction and a slightly greater inelasticity in the experiments with damaged surfaces. However, as Table 1 indicates, changes in the three coefficients were not substantial.

Bumpy Boundaries

Hanes, Jenkins and Richman[13] predicted that hemispheres affixed to infinite parallel boundaries may produce or dissipate the fluctuating energy of a rapid granular flow of smooth spheres sheared between the boundaries. They showed that the rate and direction of transfer of the fluctuating energy across this "bumpy boundary" depends on the boundary spheres' spacing, diameter and coefficient of restitution. Experimental verification of this and related theories (e.g., Jenkins and Askari[14]) therefore requires the knowledge of impact parameters for collisions involving a free sphere and another sphere rigidly affixed to a massive plate.

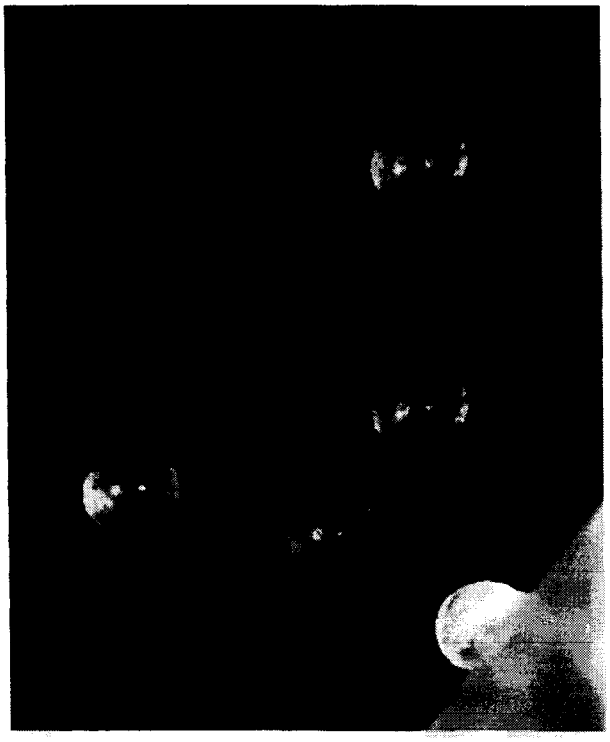

Fig. 7—Typical stroboscopic image of the collision of a free 3-mm glass bead with a similar bead rigidly affixed to a plate. In this experiment, $\Psi_1 = 0.838$ and $\Psi_2 = 0.181$

Figure 7 is a digital photograph of a typical impact between a free 3-mm glass bead and a similar bead affixed to an aluminum plate with epoxy. In these tests, our objective was to inform recent experiments of Hanes[15] with granular flows of these beads on a similar bumpy, inclined chute. For this reason, we employed Hanes's nearly spherical beads rather than perfect spheres and expected that some experimental scatter would ensue. These beads were identical to the spent beads mentioned in the previous section.

Hanes[15] anticipated that the bonding of the sphere to the plate would play an important role in determining the coefficient of restitution. In particular, he expected that the ability of the epoxy to store or to dissipate elastic energy through plastic deformations would probably affect the behavior of the impact. Thus, for this bumpy boundary, Hanes rested the sphere in a 2.2-mm hole drilled in an aluminum plate 1.3 mm thick. The plate and the sphere were then bonded to another flat aluminum plate 12.8 mm thick (Fig. 8). It is likely that this arrangement transmits the impact stresses from the glass sphere to the aluminum assembly without excessive dissipation of energy in the epoxy.

The bumpy boundary presents two principal challenges for the impact experiment. The first is that only a limited

TABLE 1—EXPERIMENTAL RESULTS

Particle Material	Collisions of	Particle Diameter (mm)	Impact Parameters			Relative Contact Velocities (m/sec)			
						|g.n|		|g.t|	
			e	μ	β_0	min	max	min	max
Polystyrene	Two spheres	4.00	0.952 ± 0.009	0.189 ± 0.009	0.46 ± 0.05	0.34	1.23	0.11	1.1
Acrylic	Two spheres	4.00	0.934 ± 0.009	0.096 ± 0.006	0.22 ± 0.07	0.35	1.25	0.07	1.14
Stainless steel	Two spheres	5.00	0.95 ± 0.03	0.099 ± 0.008	0.32 ± 0.08	0.17	1.2	0.15	1.2
Fresh glass	Two beads	2.97 ± 0.02	0.922 ± 0.021	0.048 ± 0.006	0.37 ± 0.07	0.43	1.14	0.07	1.08
Spent glass	Two beads	2.97 ± 0.02	0.972 ± 0.015	0.177 ± 0.020	0.25 ± 0.08	0.24	1.11	0.14	1.1
Fresh glass	Bead on smooth aluminum plate	2.97 ± 0.02	0.816 ± 0.013	0.131 ± 0.007	0.46 ± 0.24	0.80	1.92	0.07	1.64
Spent glass	Bead on spent aluminum plate	2.97 ± 0.02	0.800 ± 0.010	0.141 ± 0.009	0.35 ± 0.31	0.91	1.94	0.07	1.53
Spent glass	Bead on similar stationary bead	2.97 ± 0.02	0.865 ± 0.011	0.126 ± 0.014	0.34 ± 0.16	0.73	1.67	0.29	1.51

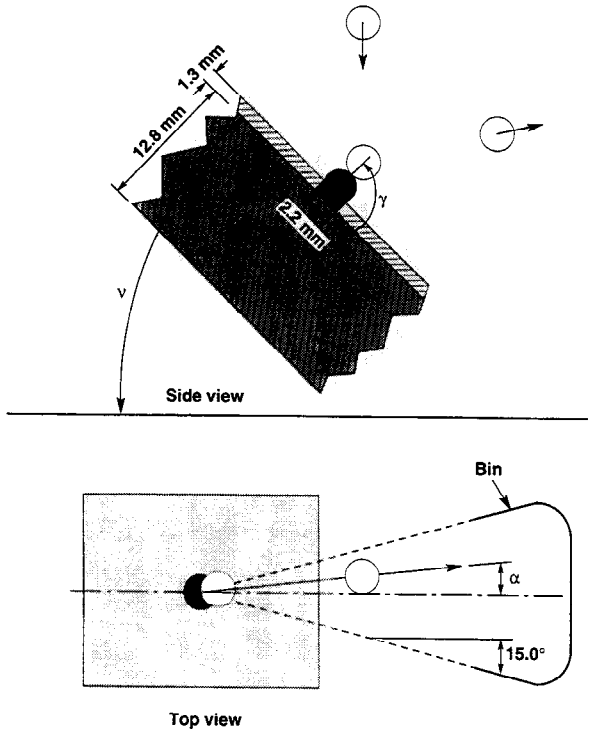

Fig. 8—Geometry of the impact on the bumpy boundary. The dimensions are shown in mm

range of incident angles produces trajectories of the rebounding sphere that do not interfere with the plate. To ensure that postcollision velocities are directed away from the plate, values of Ψ_1 in the sliding regime are limited to a relatively small range,

$$\Psi_1 = \tan\gamma \leq \cot(\theta_0 - \nu), \qquad (9)$$

where ν is the inclination of the plate and θ_0 is the smallest possible latitude of the impact point on the boundary sphere; θ_0 is a solution to the following equation:

$$\cos\nu = (1 + e)\sin(\theta_0 - \nu)\,[\sin\theta_0 + \mu\cos\theta_0]. \qquad (10)$$

In practice, the range of Ψ_1 is slightly smaller to permit the rebounding particles to describe a discernible ballistic trajectory after impact. With a horizontal plate and for typical values of e and μ, the upper bound of Ψ_1 for sliding contacts is near unity. This upper bound increases with greater inclination of the plate. Therefore, after performing a first series of impacts with the horizontal plate, we tilted the plate to the steeper inclination of $\nu = 45$ deg to extend Ψ_1 further into the sliding regime. However, at progressively steeper plate inclinations, the angular position of the impact point that generates a desired value of the incident angle γ rotates along the surface of the boundary sphere. Consequently, because two impacts at identical values of Ψ_1 but two different plate inclinations have different points of contact, they exhibit different distributions and time histories of the stress. In principle, these differences could result in different values of the collision parameters. Nevertheless, we failed to discern any trend in the data that would reveal a dependence of the coefficient of restitution on plate inclination.

The second challenge arising with the bumpy boundary is to gage the true orientation of the collision plane. In general, because perfect control of the relative positions of the particles at impact is difficult, the collision plane does not coincide exactly with the object plane of the camera. These two planes differ by an angle α (Fig. 8). For binary collisions, Foerster *et al.*[3] recorded the landing position of the two spheres on a glass stage below the impact. From this, they measured α by comparing the known projection of the camera's object plane and the line joining the landing positions of the two spheres. Then, they inferred the angle δ between $\mathbf{n}$ and the downward vertical from the apparent angle δ^* seen on the photograph using

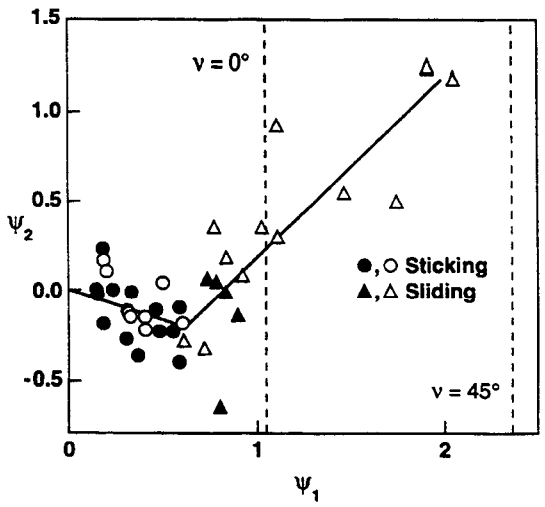

Fig. 9—Results for the impact of a free bead on the bumpy boundary of Fig. 8

$$\tan\delta = \tan\delta^* / \cos\alpha. \tag{11}$$

They noted that because the apparatus releases the spheres in vertical free-fall and without spin, **g** is aligned with the vertical, so $\gamma = \delta$. Similarly, Foerster *et al.* calculated the horizontal component c_x of the velocity of the center of mass of a sphere from its apparent value c_x^* using

$$c_x = c_x^* / \cos\alpha. \tag{12}$$

For the bumpy boundary, the analysis is identical to that of collisions of a sphere with a massive flat plate inclined at an angle $(\pi - \delta)$ from the horizontal.

Because Hanes's bumpy boundary precluded the use of a landing stage, the angle α could not be evaluated in our experiment as conveniently as in Foerster's. Instead, we constructed a bin designed to catch spheres with $|\alpha| < 15$ deg (Fig. 8), and deliberately excluded experiments that failed to capture the free sphere in the bin. The rapid processing capabilities of the digital camera made it relatively inconsequential to reject such experiments. We then analyzed valid results by assuming $\alpha = 10$ deg and evaluated the uncertainties associated with treating α as an unknown variable in the range $0 \leq |\alpha| < 15$ deg. The worst relative uncertainties in e and μ occur for glancing impacts. The corresponding errors in β_0 are negligible. At the worst, errors were 8 percent in e and 1 percent in μ; more typically, they were approximately 4 percent in e and 0.2 percent in μ.

Figure 9 presents data obtained with the bumpy boundary. There, closed and open symbols correspond to plate inclinations of 0 deg and 45 deg, respectively. The vertical dashed lines show upper bounds for Ψ_1 predicted by eqs (9) and (10) at the plate inclinations shown. Because successive measurements produce uncorrelated errors in e and μ, the average values of these parameters inferred from Fig. 9 exhibit considerably smaller uncertainties than those of individual measurements.

Summary

Impact properties are summarized in Table 1. Because they may depend on the relative velocity at contact,[16] Table 1 also lists a range for the components of that velocity. It also provides data for binary collisions of acrylic and polystyrene spheres 4 mm in diameter.

Our experiments confirm that Walton's three-parameter model is an adequate representation of the impact behavior of nearly spherical particles. However, because the model has limitations when impacts are not collinear, the reported values of the Newtonian coefficient of normal restitution should not be interpreted as a material constant for other than nearly spherical geometries. Similarly, the coefficient of tangential restitution is merely a convenient way to simplify the treatment of nearly head-on impacts. Finally, because our experience indicates that friction depends strongly on the state and history of the surface, our recommendation is for the friction coefficient to be evaluated with particles having spent a considerable time in the granular flow of interest.

Acknowledgments

The authors are indebted to W.J. Stronge, J.T. Jenkins and A. Chatterjee for stimulating discussions on the subject of impact. They are grateful to D.M. Hanes for making available a sample of the bumpy boundary used in his chute at the University of Florida. They also wish to thank Hayley Shen and Goodarz Ahmadi for supplying the plastic and steel spheres, respectively. This work was supported by the Pittsburgh Energy Technology Center of the U.S. Department of Energy under the Granular Flow Advanced Research Objective through Contract DE-AC22-91PC90183.

References

1. Jenkins, J.T., "Rapid Granular Flow," Research Directions in Fluid Mechanics, ed. J.L. Lumley, National Academy of Engineering, Washington, DC (1996).

2. Walton, O.R., "Granular Solids Flow Project," Quarterly Report UCID-20297-88-1, Lawrence Livermore National Laboratory (1988).

3. Foerster, S.F., Louge, M.Y., Chang, H. and Allia, K., "Measurements of the Collision Properties of Small Spheres," Phys. Fluids, 6, 1108–1115 (1994).

4. Dave, R.N., Yu, J. and Rosato, A.D., "Measurement of Collisional Properties of Spheres Using High-speed Video Analysis," 1993 ASME Winter Annual Meeting: Symposium on Mechatronics, **DSC-50**, *217–222 (1993).*

5. Massah, H., Shaffer, F., Sinclair, J. and Shahnam, M., "Measurements of Specular and Diffuse Particle-wall Collision Properties," Fluidization VIII: Proceedings of the Eighth International Conference on Fluidization, eds. C. Laguérie and J.-F. Large, The Engineering Foundation, New York, 641–648 (1995).

6. Maw, N., Barber, J.R. and Fawcett, J.N., "The Oblique Impact of Elastic Spheres," Wear, **38**, *101–114 (1976).*

7. Maw, N., Barber, J.R. and Fawcett, J.N., "The Role of Elastic Tangential Compliance in Oblique Impact," ASME J. Lubrication Tech., **103**, *74–80 (1981).*

8. Smith, C.E. and Liu, P.-P., "Coefficients of Restitution," J. Appl. Mech, **59**, *963–969 (1992).*

9. Smith, C.E., "Predicting Rebounds Using Rigid-body Dynamics," J. Appl. Mech., **58**, *754–758 (1991).*

10. Wang, Y. and Mason, M.T., "Two-dimensional Rigid-body Collisions with Friction," J. Appl. Mech., **59**, *635–642 (1992).*

11. Stronge, W.J., "Rigid Body Collisions with Friction," Proc. Roy. Soc. Lond. A, **431**, *169–181 (1990).*

12. Stronge, W.J., "Planar Impacts of Rough Compliant Bodies," Int. J. Impact Eng., **15**, *435–450 (1994).*

13. Hanes, D.M., Jenkins, J.T. and Richman, M.W., "The Thickness of Steady Plane Shear Flows of Circular Disks Driven by Identical Boundaries," J. Appl. Mech., **55**, *969–974 (1988).*

14. Jenkins, J.T. and Askari, E., "Boundary Conditions for Granular Flows: Phase Interfaces," J. Fluid Mech., **223**, *497–508 (1991).*

15. Hanes, D.M., private communication (1992).

16. Goldsmith, W., Impact—The Theory and Behaviour of Colliding Solids, Edward Arnold, London (1960).